JOURNAL OF SOLID STATE CHEMISTRY **121,** 443–450 (1996)
ARTICLE NO. 0061

The Structural and Magnetic Properties of $Nd_{1-x}TiO_3$ for $x = 0$, 0.05, and 0.10

G. Amow and J. E. Greedan

Department of Chemistry and Brockhouse Institute for Materials Research, McMaster University, Hamilton, Ontario, L8S 4M1 Canada

Received August 7, 1995; accepted October 26, 1995

The structural and magnetic properties of members belonging to the perovskite family, $Nd_{1-x}TiO_3$ for $x = 0$, 0.05, and 0.10, have been investigated. It is found that these compounds adopt the $GdFeO_3$-type structure belonging to the space group *Pnma*. Magnetic susceptibility measurements indicate paramagnetic Curie–Weiss behavior at temperatures typically above 100 K. Antiferromagnetic ordering of the titanium sublattice is observed at T_N of 90 and 75 K for $x = 0$ and 0.05, respectively. Investigation by low-temperature neutron diffraction reveals evidence for magnetic ordering on both the titanium and neodymium sublattices. The magnetic structure is found to be consistent with that of $PrTiO_3$ and $CeTiO_3$, having an F_xC_y configuration on the Nd^{3+} sublattice and a G_zF_x configuration for the moments on the Ti^{3+} sublattice. At 10 K, the refined magnetic moments on the Nd^{3+} sublattice are determined to be 1.11(5) and 0.99(5) μ_B and on the Ti^{3+} sublattice, 0.87(8) and 0.74(9) μ_B, for $x = 0$ and 0.05, respectively. The antiferromagnetic behavior vanishes at the $x = 0.10$ composition.

INTRODUCTION

It is well known that the rare earth titanates, $RTiO_3$, form an isostructural series of compounds whose physical properties are influenced by the size and electronegativity of the rare earth ions (1). Members belonging to this family of compounds possess the orthorhombically distorted $GdFeO_3$-type structure belonging to the space group *Pnma*. In general, these compounds are semiconducting and exhibit an impressive variety of magnetic behavior (2, 3). It has been found that $LaTiO_3$ is antiferromagnetic below 125 K, and using Bertaut's notation (4), is described as having a G_xF_z spin configuration on the titanium sublattice. Similar but more complex are $CeTiO_3$ and $PrTiO_3$, which are both antiferromagnetic below 125 K, with a magnetic structure composed of a G_xF_z spin configuration on the titanium sublattice and an F_xC_y spin configuration on the rare earth sublattice (5, 6). The weak ferromagnetic component in these magnetic structures presumably arises from a canting of the antiferromagnetic moments. For the remaining rare earth titanates, R = Gd to Tm, ferri- and ferromagnetic behavior is observed (3).

Interestingly, with such a rich variation in the magnetic properties across the titanate series, evidence for magnetic behavior and the determination of the magnetic structure of neodymium titanate, $NdTiO_3$, remained elusive. The magnetic properties of this compound were first investigated by Bazuev and Shveikin (7), who found it to be paramagnetic in the temperature range 77–450 K. Similar observations were reported by Ganguly *et al.* (8) and Maclean *et al.* (9). In addition, a low-temperature neutron study by Greedan (6) seemed to provide the most conclusive evidence for paramagnetic behavior, since measurements revealed no evidence of any magnetic ordering down to 7 K. Only recently, however, Eylem *et al.* (10) reported low field susceptibility and remanent moment measurements, which indicate that $NdTiO_3$ orders antiferromagnetically at a temperature of 90 K. Their observations were interpreted by attributing the ordering behavior to a canted antiferromagnetism on the titanium sublattice, with the assumption that the neodymium sublattice remains paramagnetic even at low temperatures. They also reported similar behavior for the calcium-doped system, $Nd_{1-x}Ca_xTiO_3$ for $0 \leq x \leq 0.2$. These observations provide the first evidence for any type of magnetic order for $NdTiO_3$, and based on this some parallels may be inferred for the $Nd_{1-x}TiO_3$ system, using the highly correlated $La_{1-x}TiO_3$ series of compounds. This system was investigated by Crandles *et al.* (11) and MacEachern *et al.* (12), whose investigations encompassed the composition range $0 \leq x \leq 0.33$. It was found that there exists a strong correlation between the structural and physical properties of the system. With regard to magnetic properties, the antiferromagnetic behavior observed for the $x = 0$ composition vanishes at $x \approx 0.08$, where paramagnetic behavior is reported. Interestingly, at this composition, the system undergoes a metal–insulating transition from the semiconducting $LaTiO_3$ to the metallic $La_{0.92}TiO_3$ and reflects the high degree of correlation in this system.

In light of the aforementioned results, the magnetic behavior of compounds belonging to the $Nd_{1-x}TiO_3$ system

0022-4596/96 $18.00

TABLE 1
Oxygen Content as Determined by Thermogravimetric Analysis

Target composition	Expected gain	Theoretical gain	Actual composition
$NdTiO_3$	3.33	3.33	$NdTiO_{3.00}$
$Nd_{0.95}TiO_3$	2.92	2.92	$Nd_{0.95}TiO_{3.00}$
$Nd_{0.90}TiO_3$	2.48	2.38	$Nd_{0.90}TiO_{3.01}$

is worth reinvestigation with low-temperature neutron diffraction. It is also interesting to determine whether or not there exists a correlation between the magnetic and electrical properties of the compositions studied.

EXPERIMENTAL PROCEDURE

Preparation of Samples

$NdTiO_3$. This composition was prepared by arc-melting stoichiometric amounts of predried Nd_2O_3 (Research Chemicals, 99.99%), TiO2 (Fisher Scientific, 99.97%), and Ti metal, according to the equation

$$Nd_2O_3 + \tfrac{3}{2}\,TiO_2 + \tfrac{1}{2}Ti \rightarrow 2NdTiO_3.$$

The powders were mixed in acetone, made into 5/8″ pellets and arc-melted together with Ti metal on a water-cooled copper hearth under 1/2 atm prepurified argon gas (99.998%).

$Nd_{0.95}TiO_3$ and $Nd_{0.90}TiO_3$. Stoichiometric amounts of Ti_2O_3 (Cerac, 99.9%) and predried Nd_2O_3 and TiO_2 were ground in acetone and made into 5/8″ pellets. The reaction is

$$\frac{(1-x)}{2}Nd_2O_3 + 3xTiO_2 + \frac{(1-3x)}{2}Ti_2O_3 \rightarrow Nd_{1-x}TiO_3$$

The pellets were sealed in a molybdenum crucible, which was placed in a tungsten induction coil, and the crucible was placed in an rf induction furnace. Preparation conditions for both compositions involved heating to 1400°C in a vacuum of approximately 10^{-4} Torr for an average of 8 to 12 hours. Phase purity determination was carried out by X-ray diffraction and on occasion the samples were reground and refired under the initial conditions to produce single-phase materials. For all three compositions, the products were black in color.

TABLE 2
Unit Cell Parameters from X-Ray Powder Diffraction

Compound	*a* (Å)	*b* (Å)	*c* (Å)	Volume (Å^3)
$NdTiO_3$	5.561(5)	7.793(8)	5.522(5)	243.22(3)
$Nd_{0.95}TiO_3$	5.592(5)	7.798(8)	5.506(4)	240.10(4)
$Nd_{0.90}TiO_3$	5.551(3)	7.796(5)	5.488(3)	237.48(2)

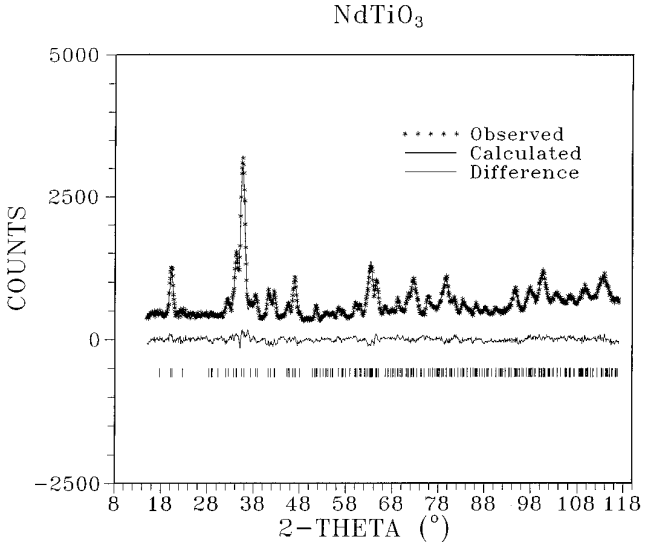

FIG. 1. Refined neutron powder profile of $NdTiO_3$.

X-Ray Powder Diffraction

Phase purity determination and initial structural characterization of the samples were carried out using a Guinier–Haag camera (IRDAB Model XDC700) with Cu$K\alpha_1$ radia-

TABLE 3
Conditions for Neutron Data Collection and Profile Refinement for Structural Determination

	$NdTiO_3$	$Nd_{0.95}TiO_3$	$Nd_{0.90}TiO_3$
2θ Range (°)	15.0–117.0	15.0–118.0	17.5–117.5
Step size (°)	0.10	0.10	0.10
No. of profile points	1021	1021	982
No. of independent reflections	254	253	251
No. of refined parameters	24	24	20[a]
R_{wp}	6.37	5.69	6.53
R_p	5.09	4.38	5.16
R_{exp}	3.94	2.95	3.24
R_{Bragg}	9.39	7.96	16.15
Goodness of fit	1.62	1.93	2.02

[a] Manual background used in refinement. $R_{wp} = 100\,\{\sum w(y_{obs} - y_{cal}/c)^2/\sum wy_{obs}^2\}^{1/2}$. $R_p = 100\sum |\,y_{obs} - y_{cal}/c\,|/\sum |\,y_{obs}|$. $R_{exp} = 100\,\{(N-P)/\sum wy_{cal}^2\}^{1/2}$. $R_{Bragg} = 100\sum |I_o - I_c|/\sum I_o$. Goodness of fit $= R_{wp}/R_{exp}$.

TABLE 4
Atomic Positions and Cell Parameters from the Profile Refinement of Neutron Powder Data Collected at Room Temperature

		$NdTiO_3$	$Nd_{0.95}TiO_3$	$Nd_{0.90}TiO_3$	$NdTiO_3$[a]
Nd	*x*	0.0598(8)	0.0437(12)	0.0374(11)	0.05412(6)
	y	0.25	0.25	0.25	0.25
	z	0.9927(13)	0.9851(22)	0.9936(22)	0.98892(5)
	B (Å^2)	0.54(7)	0.62(27)	0.236(8)	
Ti	*x*	0.5	0.5	0.5	0.5
	y	0.0	0.0	0.0	0.0
	z	0.0	0.0	0.0	0.0
	B (Å^2)	0.77(14)	1.09(43)	0.11(15)	
O1	*x*	0.4770(11)	0.4736(20)	0.4781(14)	0.4801(8)
	y	0.25	0.25	0.25	0.25
	z	0.0900(13)	0.0724(23)	0.0654(19)	0.0902(8)
	B (Å^2)	1.07(13)	2.07(55)	0.73(13)	
O2	*x*	0.3005(8)	0.3018(12)	0.2912(12)	0.2979(5)
	y	0.0501(6)	0.0524(9)	0.043(1)	0.0465(4)
	z	0.6992(7)	0.7072(14)	0.7068(13)	0.7024(5)
	B (Å^2)	0.127(77)	0.87(33)	1.35(11)	
	a (Å)	5.647(1)	5.583(4)	5.546(2)	5.589(3)
	b (Å)	7.785(2)	7.799(6)	7.798(2)	7.779(4)
	c (Å)	5.519(1)	5.489(4)	5.489(2)	5.495(3)

[a] Single crystal data from Ref. (1).

tion and silicon as an internal standard. A KEJ Instruments line scanner (Model LS20) was used to measure the positions and intensities of the diffraction lines. Unit cell constants were refined using the least-squares program LSUDF.

Thermal Gravimetric Analysis

Oxygen contents were determined by the use of a Netzsch STA Thermal Analyzer under an atmosphere of flowing air at 1000°C. A light purple powder was produced as a result of oxidation to $Nd_2Ti_2O_7$ and TiO_2. The oxygen content was calculated on the assumption of the nominal neodymium content in the target composition. The error in the experimental percent weight gain is ± 0.05.

Magnetic Susceptibility

Measurements were carried out using a Quantum Design SQUID magnetometer in the temperature range 5–300 K with an applied field of 1000 Oe. The samples used were sintered polycrystalline pellets with typical sizes of 50 mg.

Neutron Powder Diffraction

Neutron diffraction data for powdered samples were collected at the McMaster Nuclear Reactor (MNR). Neutrons of wavelength 1.3920 Å, obtained by reflection from a Cu (200) single crystal monochromator, were used in combination with a position-sensitive detector. For routine chemical structural determination the samples were placed in a thin-walled vanadium can. Measurements were made over a 2θ range of 15° to 120° at room temperature. For low-temperature measurements a thin-walled aluminum can filled with He exchange gas and sealed with an indium gasket was used. Low temperatures to 10 K were obtained using a CTI Inc. Model 21 closed-cycle refrigerator with a Cryogenics Inc. Model DRC 80C controller. Measurements were made over a 2θ range of 10° to 40° for a series of temperatures down to 20 K and an extended data set with a 2θ range of 10° to 78° was collected at 10 K for magnetic structure refinements.

STRUCTURAL CHARACTERIZATION

Thermogravimetric analysis indicated that for each compound the target composition was achieved with the oxygen stoichiometry deviating by less than 1% from the expected value of 3.00 per formula unit, assuming the nominal neodymium composition (see Table 1). Using a $GdFeO_3$-type *Pnma* model, preliminary structural determinations carried out with Guinier–Haag powder X-ray diffraction data yielded the refined unit cell parameters found in Table 2.

Structural characterization was achieved with the use of neutron diffraction data for which a typical diffraction

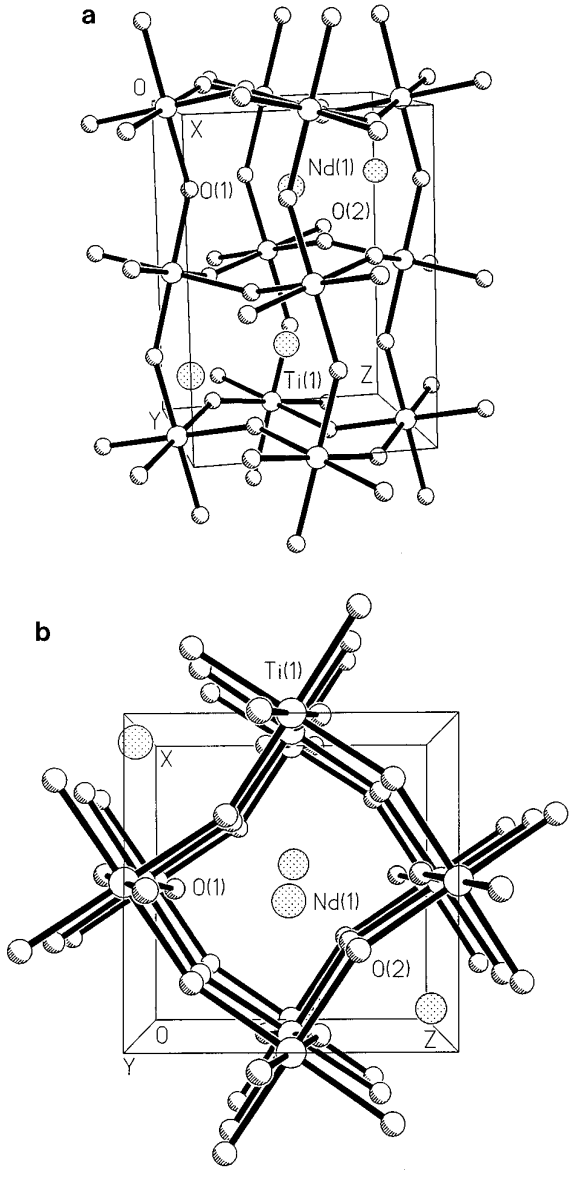

FIG. 2. (a) Perspective of *Pnma* structure and (b) view down the *b* axis.

profile can be seen in Fig. 1. Atomic positions and thermal parameters were determined by Rietveld profile refinement using the program DBWS 9600PC and the data refined smoothly in the space group *Pnma*. The results of the refinements and the refined structural parameters can be found in Tables 3 and 4, respectively. An illustration of the structure can be seen in Fig. 2. In order to accommodate the smaller sized neodymium cation, the corner-shared TiO_6 octahedra tilt along each of the *a*, *b*, and *c* axes. It is found that as the neodymium content is decreased, the tilting becomes less severe, as reflected by the Ti–O–Ti bond angles shown in Table 5.

TABLE 5
Bond Distances (Å) and Selected Bond Angles (°)

		$NdTiO_3$	$Nd_{0.95}TiO_3$	$Nd_{0.90}TiO_3$
Nd–O1	×1	2.42(4)	2.447(13)	2.476(20)
Nd–O1	×1	3.33(5)	3.219(13)	3.127(10)
Nd–O1	×1	2.350(13)	2.462(17)	2.443(16)
Nd–O1	×1	3.250(12)	3.088(18)	3.086(16)
Nd–O2	×2	2.625(24)	2.604(11)	2.656(11)
Nd–O2	×2	3.53(3)	3.484(10)	3.356(10)
Nd–O2	×2	2.717(14)	2.792(9)	2.740(9)
Nd–O2	×2	2.38(3)	2.305(10)	2.381(10)
Ti–O1	×2	2.0129(19)	1.995(3)	1.9860(20)
Ti–O2	×2	2.044(4)	1.995(7)	2.011(7)
Ti–O2	×2	2.059(4)	2.074(7)	2.003(7)
O1–Ti–O1		180.0	180.0	180.0
O2–Ti–O2		180.0	180.0	180.0
O2–Ti–O2		90.89(17)	91.9(3)	91.0(3)
		89.11(17)	88.1(3)	89.0(3)
O1–Ti–O2		87.87(23)	85.4(4)	86.8(4)
		91.13(23)	94.6(4)	93.2(4)
		89.90(22)	91.3(4)	90.8(3)
		90.10(22)	88.7(4)	89.2(3)
Ti–O1–Ti		150.4(4)	155.5(7)	158.0(6)
Ti–O2–Ti		148.40(24)	148.5(4)	152.8(4)

Similar observations were reported previously for $NdTiO_3$, based on single crystal studies (1). However, the cell parameters and bond distances reported were significantly smaller than those in Tables 4 and 5. This suggests that the previous results were for a compound whose composition had less than the desired neodymium stoichiometry of $x = 0$. Using an extrapolation and the cell volume reported, this corresponds to a neodymium content of $x \approx 0.07$, i.e., $Nd_{0.93}TiO_3$.

MAGNETIC PROPERTIES

1. Susceptibility Measurements

The temperature dependence of the magnetic susceptibility for each compound can be seen in Figs. 3a–3c. In all cases the data were corrected for core diamagnetism and above 100 K, a good fit to the Curie Weiss law could be found,

$$\chi = C/(T - \theta),$$

where C is the Curie constant, T is the temperature, and θ is the Weiss constant. The experimentally determined values of the Curie and Weiss constants can be found in Table 6. For each composition, the experimentally determined value of the Curie constant deviates from the ideal free ion value for Nd^{3+} of 1.64 emu · K · mol^{-1}. This suggests that the total susceptibility is composed of contributions from both Nd^{3+} and Ti^{3+}. It has been suggested that by

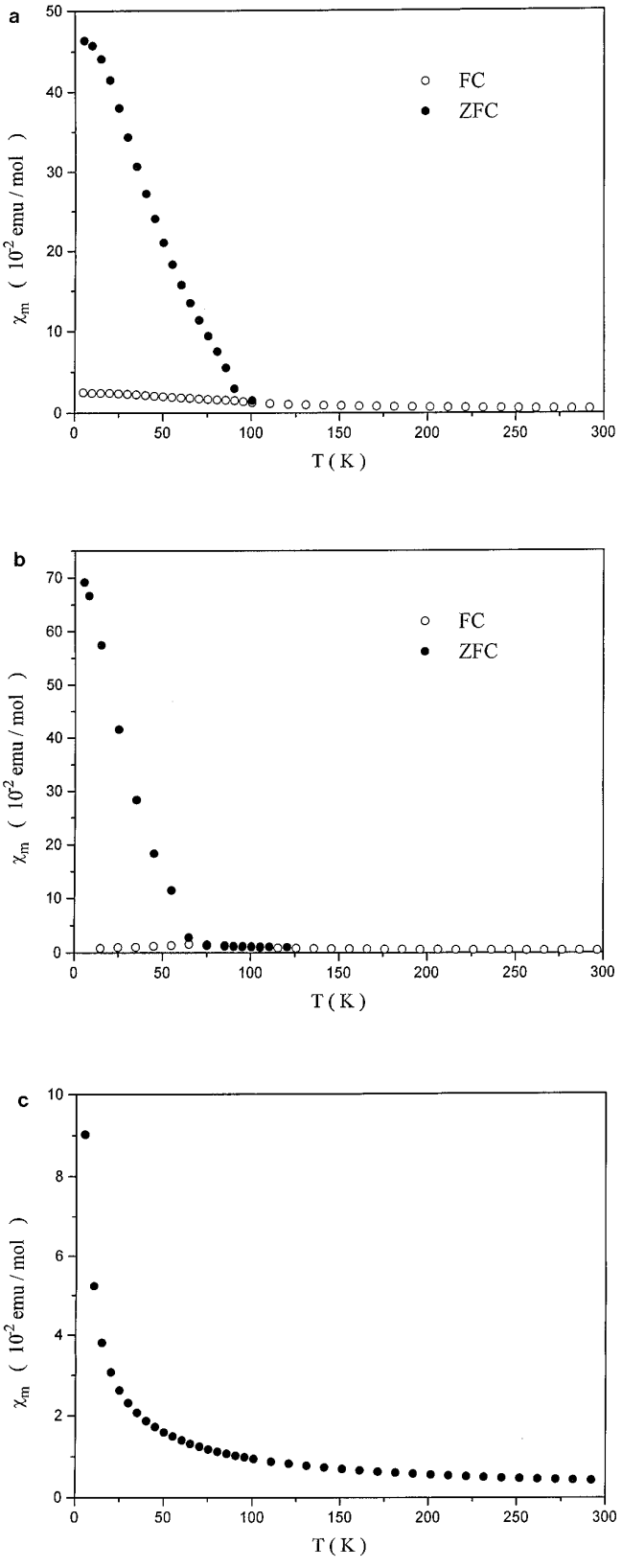

FIG. 3. Magnetic susceptibility vs temperature curves for (a) $NdTiO_3$, (b) $Nd_{0.95}TiO_3$, and (c) $Nd_{0.90}TiO_3$.

TABLE 6
Experimentally Determined Values for C, θ, and T_N

Compound	C (emu · K · mol^{-1})[a]	θ (K)	T_N (K)
$NdTiO_3$	1.71	−45.0	100
$Nd_{0.95}TiO_3$	1.49	−54.7	75
$Nd_{0.90}TiO_3$	1.58	−75.7	—

[a] Per mole of compound.

comparing $NdTiO_3$ with the isostructural $NdScO_3$ a reasonable approximation can be made (9), in order to determine the contribution from the titanium ions. However, it becomes extremely difficult to separate the individual contributions to the total susceptibility for the vacancy-doped compositions.

Below 100 K, deviation from the Curie–Weiss law is observed for all cases. This deviation can be readily explained by the crystal field splitting of the 10-fold degenerate ground state of the Nd^{3+} ion. More interesting are the divergences that are observed between the zero field and field-cooled measurements for $NdTiO_3$ and $Nd_{0.95}TiO_3$ at 100 and 75 K, respectively, which suggests the onset of some type of magnetic order. This compares favorably with the ordering temperature of 90 K reported by Eylem *et al.* (10) for the $x = 0$ case. No divergences between the zero field and field-cooled measurements were observed for $x = 0$ case. No divergences between the zero field and field-cooled measurements were observed for $x = 0.10$, indicating the absence of magnetic order for this composition.

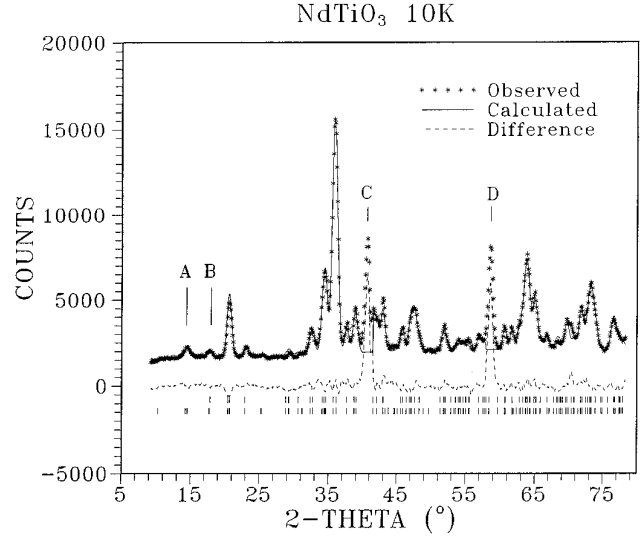

FIG. 4. Refined neutron powder data taken at 10 K for $NdTiO_3$. Magnetic peaks are labeled A (100,001) and B (110,011). The peaks labeled C and D are due to aluminum and were excluded in the refinement.

TABLE 7

Conditions and Refinement Results for the Combined Chemical and Magnetic Structures for $NdTiO_3$ and $Nd_{0.95}TiO_3$ at 10 K

2θ range (°)	9.0–78.0	10.0–75.0
Step size (°)	0.10	0.10
No. of profile points	691	651
No of refined parameters	21	21
	Chemical cell	
R_{wp}	6.19	5.96
R_{exp}	1.82	2.30
R_{Bragg}	8.30	8.36
Goodness of fit	3.40	2.60
	Magnetic cell	
R_{Magn}[a]	29.9	26.9
Moment configuration		
Nd^{3+}	F_xC_y	F_xC_y
Ti^{3+}	G_zF_x	G_zF_x
Magnetic moment		
Nd^{3+}	1.11(5) μ_B	0.87(8) μ_B
Ti^{3+}	0.99(5) μ_B	0.74(9) μ_B

[a] Magnetic R factor.

2. *Low-Temperature Neutron Diffraction Measurements*

Low-temperature neutron diffraction measurements were carried out using powdered samples of $NdTiO_3$ and $Nd_{0.95}TiO_3$ for a series of temperatures below which ordering is observed in the susceptibility measurements. The data collected at 10 K for both $x = 0$ and 0.05 show the emergence of two well-defined peaks of low intensity occurring at 2θ values of ~14° and ~17°, respectively; see Fig. 4. The profiles bear a striking resemblance to those obtained for both $CeTiO_3$ and $PrTiO_3$ for which the magnetic structures were solved to yield a G_zF_x configuration for the Ti^{3+} moments and an F_xC_y configuration for the Ce^{3+} and Pr^{3+} ions (5, 6). Consequently, the peak at ~14°, A, is assigned the (100,001) reflection and is C type in Bertaut's notation and the peak at ~17°, B, is indexed as (110) which is G type. The latter overlaps the (011) reflection, which is allowed in *Pnma*. The magnetic structures were refined using the program FULLPROF (13). For the refinements at low temperatures, the overall temperature factor was fixed at $B = 0.25$ Å^{-2}, due to the strong correlation with the refined moments, especially at the titanium sites. The results for each composition are discussed separately below.

(*a*) *$NdTiO_3$*. The results of a combined magnetic and chemical structure for both $NdTiO_3$ and $Nd_{0.95}TiO_3$ at 10 K are shown in Tables 7 and 8, with the profile fit for $NdTiO_3$ displayed in Fig. 4. The model for the magnetic structure is a G-type configuration for the Ti^{3+} moments and a C-type configuration for the Nd^{3+} moments. The values for the refined moments are reasonable for both ions at 10 K.

Refinements were also done at several temperatures above 10 K for both samples using less extensive data sets. In these cases the half-width parameters were fixed along with the overall temperature factor. The results for $NdTiO_3$ are plotted in Figs. 5a and 5b. The temperature dependence of the Ti^{3+} moment, Fig. 5b, is consistent with an ordering temperature of 90 K as found from the susceptibility data. Because of the restricted conditions under which the refinements were carried out, the temperature dependence was checked by a second method which involved simply fitting the (110,011) doublet to a Gaussian lineshape for each temperature with no reference to a structural model. The temperature dependence of the square root of these intensities is essentially the same as that in Fig. 5b.

The thermal development of the Nd^{3+} moment which is associated with the (100,001) peak is rather different, as seen in Fig. 5a. There is a sharp decline from a low-temperature value of ~1.10(1) μ_B between 10 and 20 K to a roughly constant value of 0.56(9) μ_B at 50 K and above. This is essentially the same type of temperature dependence seen for $PrTiO_3$ and can be explained as a polarization of the Nd^{3+} moments by the coupling to the Ti^{3+} sublattice (6).

Further insight concerning the nature of the ordering on the Nd^{3+} sublattice is seen in Figs. 6a and 6b, where the full width at half-maximum, FWHM, for both sets of magnetic reflections, A (100,001) and B (110,0011), are shown. For B, Fig. 6b, the peak width is essentially constant

TABLE 8

Atomic Positions and Cell parameters from the Refinement of the Combined Chemical and Magnetic Structure of $NdTiO_3$ and $Nd_{0.95}TiO_3$ at 10 K

		$NdTiO_3$	$Nd_{0.95}TiO_3$
Nd	x	0.065(1)	0.0541(9)
	y	0.25	0.25
	z	0.9814(13)	0.9849(15)
Ti	x	0.5	0.5
	y	0	0
	z	0	0
O1	x	0.4871(13)	0.4853(14)
	y	0.25	0.25
	z	0.0931(16)	0.0875(17)
O2	x	0.299(1)	0.298(1)
	y	0.0480(7)	0.0438(8)
	z	0.695(1)	0.6969(11)
	a (Å)	5.600(2)	5.571(2)
	b (Å)	7.752(2)	7.777(2)
	c (Å)	5.504(2)	5.492(2)

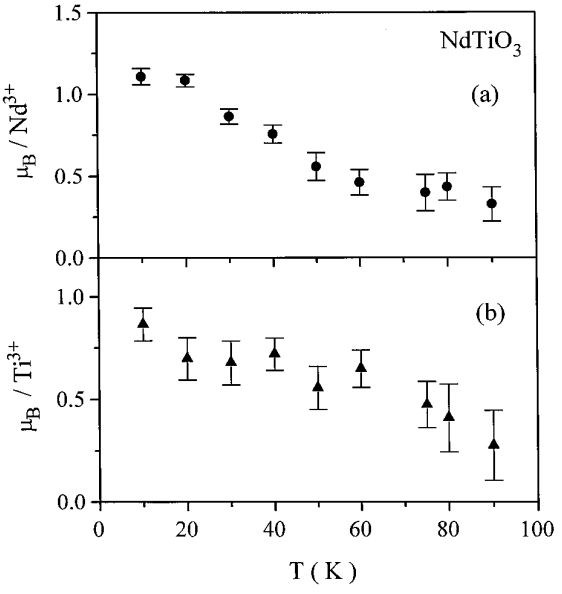

FIG. 5. Magnetic moment vs temperature curves for $NdTiO_3$ (a) Nd^{3+} and (b) Ti^{3+}.

at about 0.88° as a function of temperature. The small increase near 90 K may reflect the presence of subcritical clusters on the Ti^{3+} sublattice. The point at 200 K represents the (011) reflection which is not magnetic in origin, but is at essentially the same position as the (110) magnetic component. Very different behavior is seen for A, Fig. 6a, where the FWHM increases from a constant value of 1.15(5)° at low temperatures to values approaching 2.24(32)° by 50 K. An estimation of the correlation length can be obtained from the expression

$$\xi = 1/[\Gamma^2_{EXP} - \Gamma^2_{RES}]^{1/2},$$

where ξ is the correlation length in Å, and Γ_{EXP} and Γ_{RES} are the experimentally determined and expected resolution-limited Gaussian FWHMs, respectively. Taking into account the changes to the peak width as a function of position on the linear tube detector, the resolution-limited linewidth at 14.20° is 0.91°. The observed linewidths clearly exceed the resolution-limited value at all temperatures. Correlation lengths, determined to be 18(3) Å at 10 K and 6(1) Å at 50 K, indicate that the order on the Nd^{3+} sublattice is of short range in the temperature regime investigated, extending over only a few unit cells.

The inhibition of true long-range order on the Nd^{3+} sublattice can be attributed to the symmetry cancellation or frustration effects which arise from the crystal geometry. The Nd^{3+} moment is roughly in the center of a slightly distorted primitve cube with eight nearest Ti^{3+} neighbors, four with one spin direction and four antiparallel to these. Note that in Figs. 6a, values for the FWHM are reported out to 200 K and that the values for the Nd^{3+} moment remain finite even at temperatures exceeding T_N for the Ti^{3+} sublattice ordering. Both results arise from the observation of a very broad (FWHM ~2.5°) weak feature at the expected position for the (100,001) magnetic peak. While the persistence of this broad peak out to such high temperatures could indicate the presence of short-range magnetic order, this would be very unusual and it is more likely to due to an anomaly in the background. In any case, nothing definitive can be stated with the current data and this matter will be studied further.

(*b*) $Nd_{0.95}TiO_3$. The results for this material parallel those for $NdTiO_3$ but on a slightly lower temperature scale, as seen in Figs. 7 and 8. The thermal development of the Ti^{3+} moment is consistent with $T_N \sim 75$ K from the susceptibility data and the linewidths are in the resolution-limited range. The Ti^{3+} ordered moment is somewhat smaller than that found for $NdTiO_3$ at 10 K.

The behavior of the Nd^{3+} sublattice moment, Fig. 7b, indicates a gradual increase beginning at about 40 K. The two points at 60 and 70 K are at the detection limit, as indicated by the large error bars. The broad, temperature robust feature at the (100,001) position found for $NdTiO_3$ was not observed above 70 K for $Nd_{0.95}TiO_3$, which casts further doubt on its significance in the former material. From the linewidths, Figs. 8a, it is seen that the Nd^{3+} sublattice order is only of short range as in $NdTiO_3$.

SUMMARY AND CONCLUSIONS

Members belonging to the solid solution $Nd_{1-x}TiO_3$, $x = 0$, 0.05, and 0.10, adopt the $GdFeO_3$-type structure.

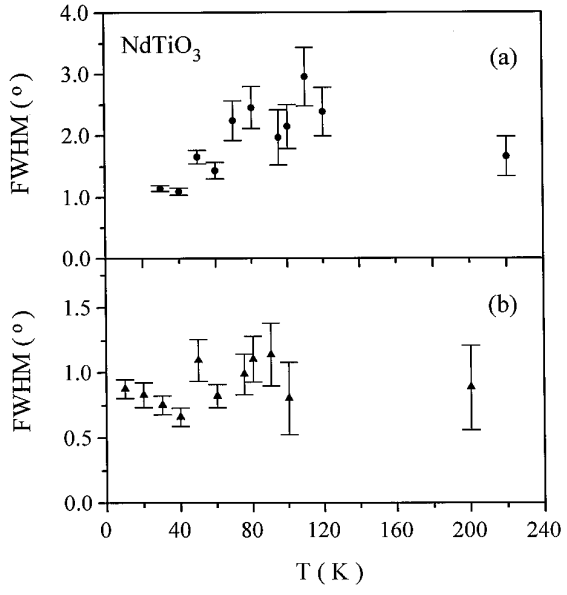

FIG. 6. Full width at half-maximum (FWHM) vs temperature for $NdTiO_3$ (a) A (100,001) and (b) B (110,011) reflections.

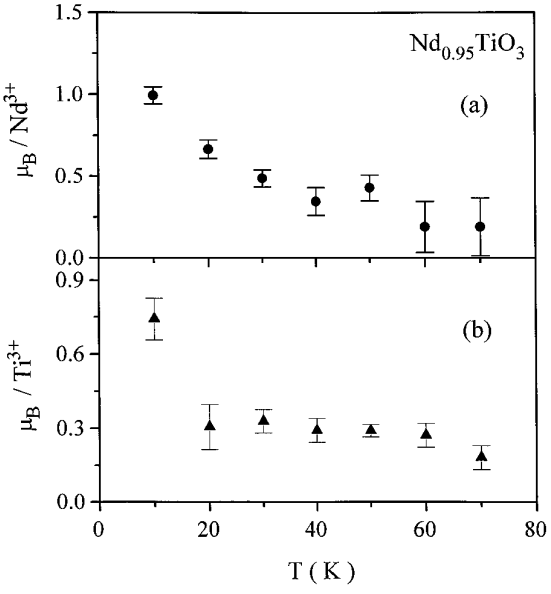

FIG. 7. Magnetic moment vs temperature for $Nd_{0.95}TiO_3$ (a) Nd^{3+} and (b) Ti^{3+}.

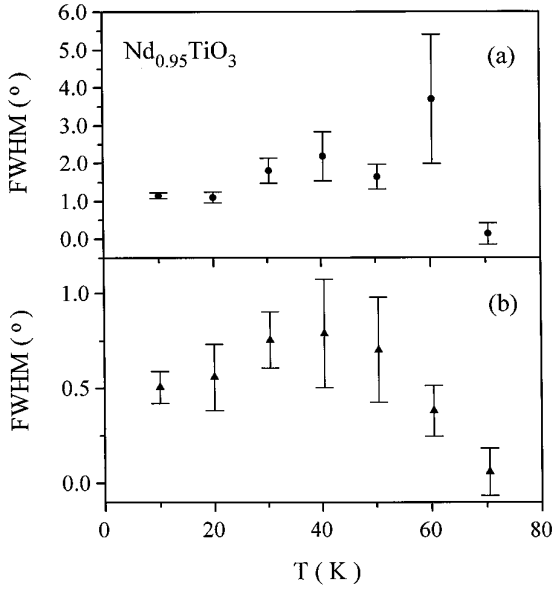

FIG. 8. Full width at half-maximum (FWHM) vs temperature for $Nd_{0.95}TiO_3$ (a) A (100,001) and (b) B (110,011) reflections.

The results reported here suggest that the composition used in the previous low-temperature neutron diffraction study by Greedan (6) contained less than the nominal composition of neodymium, i.e., $x \sim 0.07$. This seems to be the most likely explanation for the nonobservance of any type of magnetic behavior for this composition. It is found that for reasonably stoichiometric compositions, antiferromagnetic behavior on both metal ion sublattices is observed in compositions with $x = 0$ and 0.05. The ordering on the Nd^{3+} sublattice is of short range but is clearly evident and is in sharp contrast to the paramagnetic behavior assumed by Eylem *et al.* (10). The magnetic structure has been determined to be similar to that of $CeTiO_3$ and $PrTiO_3$, where there is a F_xC_y configuration on the Nd^{3+} sublattice and a G_zF_x configuration on the Ti^{3+} sublattice. The antiferromagnetic behavior is observed to vanish on approaching the $Nd_{0.90}TiO_3$ composition. This observation appears to be consistent with those made for the $La_{1-x}TiO_3$ series of compounds, where the antiferromagnetic behavior vanishes as metallic behavior is encountered. It is well known that $NdTiO_3$ is semiconducting, and it is found that this behavior extends to the $x = 0.05$ composition. As part of a larger body of work to be published in the future, evidence will be presented that the $x = 0.10$ composition exhibits an unusual and interesting resistivity behavior. It is clear, however, that the semiconducting behavior vanishes at this composition.

REFERENCES

1. D. A. MacLean, H. N. Ng, and J. E. Greedan, *J. Solid State Chem.* **30,** 35 (1979).
2. G. V. Bazuev and G. P. Shveikin, *Inorg. Mater.* **19,** 92 (1983).
3. J. E. Greedan, *J. Less-Common Met.* **111,** 335 (1985).
4. E. F. Bertaut, *in* "Magnetism" (G. T. Rado and H. Suhl, Eds.), Vol. III, p. 149. Academic Press, New York, 1963.
5. J. P. Goral and J. E. Greedan, *J. Magn. Magn. Mater.* **37,** 315 (1983).
6. J. E. Greedan, *J. Magn. Magn. Mater.* **44,** 299 (1984).
7. G. V. Bazuev and G. P. Shveikin, *Inorg. Mater.* **22,** 1185 (1986).
8. P. Ganguly, O. Parkash, and C. N. R. Rao, *Phys. Status Solid A* **36,** 669 (1976).
9. D. A. Maclean, K. Seto, and J. E. Greedan, *J. Solid State Chem.* **40,** 241 (1981).
10. C. Eylem, H. L. Ju, B. W. Eichorn, and R. L. Green, *J. Solid State Chem.* **114,** 164 (1995).
11. D. A. Crandles, T. Timusk, J. D. Garrett, and J. E. Greedan, *Phys. Rev. B* **49**(23), 16,207 (1994).
12. M. J. MacEachern, H. Dabkowska, J. D. Garrett, G. Amow, W. Gong, G. Liu, and J. E. Greedan, *Chem. Mater.* **6,** 2092 (1994).
13. J. Rodriguez-Carvajal, "FULLPROF: A Program for Reitveld Refinement and Pattern Matching Analysis," Abstracts of the Satellite Meeting on Powder Diffraction on the XV Congress of the International Union of Crystallography, p. 127, Toulouse, France, 1990.